Singlet oxygen generation efficiency and antimicrobial ability in glutathione protected Ag31 nanoclusters

Hao Yuan, Mary Theresa, Dipankar Bain, Hussein Fakhouri, K Sreekanth, Aswani Ravi, Sabu Thomas, Nandakumar Kalarikkal, Rodolphe Antoine, E.K. Radhakrishnan

Singlet Oxygen Generation Efficiency and Antimicrobial Ability in Glutathione Protected Ag_{31} Nanoclusters

Hao Yuan[1], Mary Theresa[2], Dipankar Bain[1], Hussein Fakhouri[1], Sreekanth K[2], Aswani Raveendran[2], Sabu Thomas[3], Nandakumar Kalarikkal[4], Rodolphe Antoine[1,*], and Radhakrishnan E.K.[2,*]

[1] Institut Lumière Matière UMR 5306, Université Claude Bernard Lyon 1, CNRS, Univ Lyon, F69100 Villeurbanne, France

[2] School of Biosciences, Mahatma Gandhi University, P.D Hills (P.O), Kottayam, Kerala, 686 560, India

[3] School of Applied Physics, Mahatma Gandhi University, P.D Hills (P.O), Kottayam, Kerala, 686 560, India

[4] School of Chemistry, Mahatma Gandhi University, P.D Hills (P.O), Kottayam, Kerala, 686 560, India

Corresponding Author

*RA : rodolphe.antoine@univ-lyon1.fr, *REK : radhakrishnanek@mgu.ac.in*

Abstract:

Ligand protected silver nanoclusters (Ag NCs) have recently been reported to have significant applications as antimicrobial agents. In the current study, glutathione (SG) protected silver nanocluster was synthesized leading to $Ag_{31}SG_{19}$ by cyclic reduction and oxidative condition and was evaluated for its singlet oxygen generation and antibacterial activity. From the results of the study, $Ag_{31}SG_{19}$ was found to have inhibitory activity against *Escherichia coli* and *Staphylococcus aureus* with a diameter of 15.3 ± 0.58 mm and 16.7 ± 0.58 mm respectively. The MIC was also calculated to have 0.3125 mg/ml and 0.1562 mg/ml respectively. In addition, the $Ag_{31}SG_{19}$ was found to have high efficiency for the generation of singlet oxygen. Based on the results of the study, the antimicrobial mechanisms of $Ag_{31}SG_{19}$ could be predicted to be mainly because of the generation of singlet oxygen species in addition to the activity due to the release of Ag^{+} ions from the nanoclusters. These multimechanistic antimicrobial effects make the synthesized $Ag_{31}SG_{19}$ to be a promising candidate for a broad range of antimicrobial applications.

Keywords:

silver nanoclusters; antimicrobial agent; quantum clusters; reactive oxygen species

Highlights:

- Good photostability of $Ag_{31}SG_{19}$ nanoclusters was revealed.
- $Ag_{31}SG_{19}$ nanoclusters showed a higher efficiency for $^{1}O_{2}$ production compared with new methylene blue under 473 nm irradiation.
- Enhanced antibacterial activity of $Ag_{31}SG_{19}$ nanoclusters compared to previous works was presented.

Introduction

Bacterial infections have caused serious threat to human health with massive global economic loss.[1] Even though antibiotics are being considered as the most effective antibacterial medicine, their widespread use has already resulted in the development of antimicrobial resistance (AMR) among microbial pathogens.[2] Here is the relevance of exploring nanotechnological advances for the discovery of new nanoscale materials with high antimicrobial efficiency and safety.[3, 4] Nanomaterials generally cause the generation of reactive oxygen species (ROS) and hence exhibit potential antibacterial activity. The targeted killing action of nanomaterials against pathogenic bacteria hence could be due to the ROS which act as strong oxidants leading to oxidative damage of cellular constituents.[5, 6]

Among the various nanomaterials, ligand protected noble metal nanoclusters (NCs) are novel entities having a well-defined number of metal atoms and ligands.[7-9] When protected by the biomolecular templates, the nanoclusters can exhibit strong luminescence with good biocompatibility, which make them highly appealing as theranostic probes for biomedical applications.[10-14] More importantly, NCs can exhibit their long triplet-state lifetime and the singlet oxygen ($^1O_2$), the most damaging ROS species against microorganisms, has been reported to be generated by the energy transfer from NCs to molecular oxygen upon light irradiation.[15, 16] Indeed, as illustrated in Scheme S1 (in supporting materials), an efficient photosensitizer for $^1O_2$ production requires a high triplet-state yield with a triplet-state energy larger than the energy of $^1O_2$ (0.98 eV) for efficient energy transfer to $^3O_2$. From this viewpoint, the optical gap of thiolate protected silver nanoclusters is usually higher than 1 eV and since presenting long-lifetime, the triplet-state efficiency is high.[17] Consequently the nanoclusters have also been observed to display antibacterial capability after being metabolized by the bacterial cells.[18-20] In addition to their high capability to generate ROS, the antimicrobial mechanisms of metal NCs may also include the cell wall and membrane disruption, damage to intracellular components. In the case of silver-based NCs, due to their moderate stability the antimicrobial mechanisms also involve release of metal ions.[21-23] Thus for the ultrasmall Ag^+-rich nanoclusters, it has been proposed to have both efficient

ROS generation and abundant Ag^+ ions on its surface resulting in enhanced antibacterial activity.[24]

Compared with the AgNPs, ultrasmall AgNCs can have higher surface to volume ratio which make them to be more susceptible to the oxidative dissolution resulting in a fast release of Ag^+ and thereby enhanced antibacterial performance. In a previous study, glutathione (GSH)-protected silver nanoclusters which have been produced mainly as mixture ($Ag_n(SG)_m$) [19, 25] were reported to have strong activity against *Pseudomonas aeruginosa* due to the easily oxidized and released Ag^+ on the surface of AgNCs. It has been reported by Yuan et al. that the ultrasmall Ag^+-rich nanoclusters (GSH-capped Ag^+-rich Ag NCs) can have higher antibacterial activity when compared with the neutral Ag-rich counterpart.[24] Even though preliminary mass spectrometry data were reported in previous studies, insights into atomic precision for the silver cluster synthesis was not enough to explore its structure–activity relationship. Based on a facile aqueous-based synthesis,[26] the current study demonstrated the synthesis of Ag nanoclusters ($Ag_{31}SG_{19}$) using glutathione as thiolate ligand. Stability and photo-induced ROS efficiency of Ag NCs are explored and compared with ultrasmall Ag nanoparticles. Also their antimicrobial capabilities are reported.

2 Experimental Section

2.1 Materials

All chemicals were purchased and used directly without purification. Silver nitrate ($AgNO_3$), (±)-α-lipoic acid, tetramethylammonium borohydride ($((CH_3)_4N(BH_4)$), sodium borohydride ($NaBH_4$), trisodium citrate (TSC), 1,3-diphenylisobenzofuran (DPBF), sodium hydrate (NaOH), and 2,7-dichlorodihydrofluorescein diacetate (H_2DCF-DA) were purchased from Sigma Aldrich. L-glutathione (GSH) reduced were procured from Carl Roth. Ammonia (NH_4OH), diethyl ether, and ethanol were purchased from VWR Chemicals. Methanol was purchased from Honeywell. New methylene blue (NMB) was purchased from TCI. Ultrapure Milli-Q water (resistivity 18.2 MΩ) was used for for all of the experiments.

2.2 Instrumentation

Electrospray ionization mass spectra (ESI-MS) of silver nanoclusters were recorded on a Thermo Fisher LTQ-Velos linear ion trap mass spectrometer (mass reolution ~7500). UV−Vis absorption spectra were analysed using Avantes AvaSpec-2048 spectrophotometer with an AvaLight DH-S deuterium lamp. Transimission electron microscopy (TEM) images were obtained using a JEOL JEM 2100 microscope. Fluorescence emission spectra were studied using a Horiba FluoroMax-4 spectrophotometer and fluorescence lifetimes were measured using custom-built set-up[27].

2.3 Synthesis of atomically precise silver nanoclusters

Two atomically precise silver nanoclusters were sythesized as our previous reports with some modification. For $Ag_{31}SG_{19}$ synthesis, the procedures of cyclic reduction under oxidative conditions were the same as previous synthesis[17]. Here, in a dark environment, 1 mL of $AgNO_3$ solution (55 mg/mL) was dropwise added to an solution of L-glutathione (200 mg in 35 mL of H_2O) under ice-water bath. Further to this, 800 mL of 1 M NaOH solution was added to adjust the final pH to 6~7. Then, under constant stiring, 36 mg of $NaBH_4$ in 1 mL of ice-cold water was quickly added. After 1.5 h stiring, 300 mL of hydrogen peroxide (33%) was further added to the dark brown solution. Then, 140 mL $AgNO_3$ solution (100 mg/mL) and 50 mg GSH were added after 30 min. This was followed by the addition of 500 mL of ice-cold solution of $NaBH_4$ (20 mg/mL) after 5 min. The reaction mixture was kept stirring vigorously for 1.5 h till to a brown-red solution was obtained. For purification, the solution was evaporated to ~5 mL using a rotary evaporator at 30℃. This was further precipitated with the addition of 15 mL methanol followed by centrifugation. The precipitate was further dissolved in 20 mL H_2O followed by the addition of 50 ml of glacial acetic acid. This was kept still for 2 h before centrifugation at 13 000 rpm for 30 min. The precipitate was further removed and the supernatant was further concentrated by evaporator and precipitated with methanol. Then the powder was washed with methanol/diethyl ether for 3 times and dried.

The $Ag_{29}DHLA_{12}$ was synthesized as per the method described previously[28] with some modification. Here, 100 mg of (±)-α-lipoic acid was dissolved in a mixture of 5 ml methanol and 10 ml water. Then, 85 mg of sodium borohydride was added and the solution was stirred for 30 min to reduce the lipoic acid. Then, excess reducer

was eliminated by sonication for 1 hour. Further to this, 41 mg of silver nitrate (dissolved in 15 mL of water) was added rapidly, followed by the addition of 1 ml of 10% NH_4OH solution. The solution was further heated at 50 °C and 85 mg of sodium borohydride was added again. After 1 hour, 42.5 mg of sodium borohydride was added further when the color became bright orange. After 1 hour, the solution was concentrated using a rotary evaporator. Then, 5 mL of ethanol and 20 mL of diethyl ether were added and was followed with the addition of 50 μL of glacial acetic acid. This was then centrifuged for 5 minutes at 9000 rpm, the precipitate was collected, washed first with ethanol/diethyl ether and then with diethyl ether. The brown powder obtained was dried by natural evaporation.

2.4 Synthesis of ultra-small 5-nm silver plasmonic nanoparticles.

The silver plasmonic nanoparticles were synthesized as per the methods reported by Agnihotri et al.[29] Here, freshly prepared $NaBH_4$ aqueous solution (2 mM, 24 mL) was added to trisodium citrate (TSC) aqueous solution (4.28 mM, 24 mL). The mixture was heated at 60 °C for 30 mins under vigorous stirring in dark. Then, 2mL of $AgNO_3$ solution (1 mM) was added drop-wise following with increase of temperature to 90 °C. When temperature was raised to 90 °C, the pH was also adjusted to 10.5 with the addition of 0.1 M NaOH. After heating for 30 minutes, the light-yellow solution was cooled down at room temperature. This silver nanoparticle solution was characterized by absorption spectroscopy, and by transimission electron microscopy (TEM). The concentration of AgNPs was verified using the absorption coefficient of 1.9×10^3 M^{-1} cm^{-1} (for 6 nm AgNPs has reported by Mulvaney et al.[30]) at plasmonic peak of ~394 nm according to Lambert-Beer law.

2.5 Reactive oxygen species (ROS) generation measurements

2.5.1 Protocol for $^1O_2$ generation measurements

The singlet oxygen generation efficiency was measured by an indirect method with the $^1O_2$ sensor of 1,3-diphenylisobenzofuran (DPBF).[16] Singlet oxygen generation was monitored under the excitation at 473 nm using a continuous wavelength laser (Changchun New Industries Optoelectronics Tech. Co., Ltd, China) with an output power of 250 mW and a beam diameter of 3 mm. A 532 nm continuous wavelength laser (Spectra-Physics) with an output power set to 282 mW (beam diameter: 3 mm) was also used for the comparison. A typical solution used in the experiment contained nanoclusters/nanoparticles/dyes and DPBF with a

concentration of 1.37 × 10^{-6} M and 6.15 × 10^{-5} M, respectively. All solutions were prepared in ethanol. For Ag NPs, the mixure solution with ethanol-water solvent (50/50 in volume ratio) was used. The samples were loaded in quartz cuvettes (1cm light path length) and the absorbance was were recorded with irradation for different time.

2.5.2 Statistical analysis for $^1O_2$ generation rate

The concentration of DPBF was calculated from the intensity of absorption peak at 410 nm according to Beer–Lambert law. The rate of $^1O_2$ generation was obtained by the initial DPBF concentration change over time by a function:

$$rate\ of\ {}^1O_2\ \ generation = \frac{c[DPBF]_{0min} - c[DPBF]_{5min}}{\Delta t} / c[NCs]$$

$c[DPBF]_{0min}$ and $c[DPBF]_{5min}$ represent the concentration of DPBF at 0 min and 5 min under irradiation, respectively. Δt represents the time under irradiation (5 mins), and $c[NCs]$=1.37 × 10^{-6} M. The photoluminescence lifetime was calculated by two-exponential fitting in the decay curve. The uncertainty was evaluated by measuring 3 times repeatly.

2.5.3 Protocol for oxidants generation indication

An excellent oxidants fluorescent indicator, 2′,7′-dichlorodihydrofluorescein (H_2DCF) was used for marking the generation of reactive oxygen species, including superoxide (•O_2^-), hydroxyl radical (•OH), and hydrogen peroxide (H_2O_2).[31, 32] H_2DCF can be oxidized to green fluorescent 2′,7′-dichlorofluorescein (DCF) with an emission peak at ~525 nm. The ROS generation can be indicated by the fluorescence change on fluorescence spectra.

The commercial dye 2,7-dichlorodihydrofluorescein diacetate (H_2DCF-DA) was firstly prepared based on reported procedure[33]: 0.5 mL of 2 mM H_2DCF-DA in ethanol was added to 2.0 mL of 10 mM NaOH and stilled for 30 mins at room temperature under darkness. Then Dulbecco's phosphate-buffered saline (DPBS, pH7.2, without calcium, magnesium, Thermo Fisher Scientific) was added to a finial concentration at 123 μM. Freshly prepared H_2DCF solution was used for further.

For oxidants generation indication, 2 mL mixture aqueous solution containing prepared H_2DCF (6.15 × 10^{-5} M) and $Ag_{31}SG_{19}$ (1.37 × 10^{-6} M) was irridiated for 10

mins under the excitation of 473 nm continuous wavelength laser. Before and after laser irradiation, fluorescence emssion spectra were recorded with excitation wavelength at 488 nm.

2.6 Antibacterial activity analysis of $Ag_{31}SG_{19}$ and plasmonic AgNPs

The antibacterial activity of $Ag_{31}SG_{19}$ and plasmonic AgNPs was studied against Gram-positive *Staphylococcus aureus* (MTCC 96) and Gram-negative *Escherichia coli* (ATCC 35218) by both agar well diffusion and minimum inhibitory concentration.

2.6.1 Agar well diffusion analysis

The antibacterial activity of $Ag_{31}SG_{19}$ and plasmonic AgNPs was evaluated against *E. coli* and *S. aureus* by the standard well diffusion method in Mueller Hinton Agar (MHA) plates by following the Clinical and Laboratory Standards Institute (CLSI) guidelines (CLSI M02-A13). For this, a 20 mg/ml suspension of $Ag_{31}SG_{19}$ was prepared. Here, the bacterial inoculum was prepared by adjusting the cell concentration of respective cultures to 1.5 x 10^8 CFU/ml (0.5 McFarland) and the organisms were inoculated onto the MHA plates as lawn culture. Then, wells were cut on the media and 60 µl of $Ag_{31}SG_{19}$ suspension was added to each well. Plates were further incubated at 37℃ for 24 hours and the diameter of the zone of inhibition was measured using a zone measuring scale and the experiment was carried out in triplicates. The antimicrobial experiment was conducted under visible light exposure (400-700 nm) in Biosafety cabinet level 2.

2.6.2 The Minimum Inhibitory Concentration analysis

The Minimum Inhibitory Concentration (MIC) is defined as the lowest concentration of the antimicrobial agent that can inhibit the growth of bacteria. MIC of $Ag_{31}SG_{19}$ against *S. aureus* and *E. coli* was evaluated by using the standard broth microdilution method as per the CLSI guidelines (CLSI M07-A10). For this, the test organisms were incubated overnight at 37°C in Muller Hinton Broth (MHB) and inoculum was prepared as described above. Further, serial dilution was carried out to obtain different concentrations of $Ag_{31}SG_{19}$ (5, 2.5, 1.25, 0.625, 0.3125, 0.1563, 0.0781, 0.0391, 0.0195, 0.0098, 0.0049, and 0.0024 mg/ml) in a 96-well microtiter plate and each well was further inoculated with 100 µl of the selected test organisms. The plate was then incubated under shaking conditions at 100 rpm and 37℃ for 24 hours. After this, 0.01% Resazurin dye (30µl) was added to each of the well followed

by incubation in dark for 30-45 mins. MIC value of $Ag_{31}SG_{19}$ against each organism was identified based on the colour change observed with the addition of Resazurin. Both sterility and growth controls were also maintained and the experiment was carried out in triplicates.[34]

Results

3.1 Characterization of atomically precise $Ag_{31}SG_{19}$ silver nanoclusters and their (photo)stability.

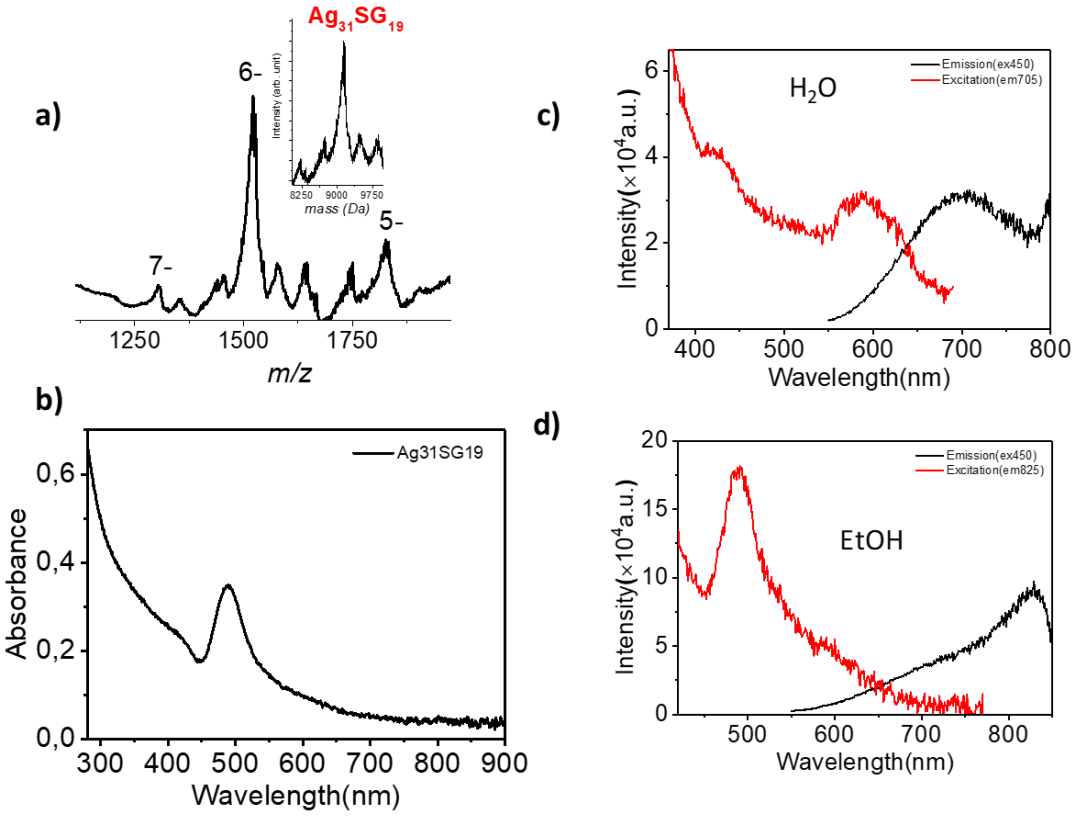

Figure 1 Mass spectrometry (a) and optical (b-d) characterization of $Ag_{31}SG_{19}$. (a) ESI-MS spectrum recorded in the negative mode of ionization. Inset : Deconvoluted ESI-MS spectra. (b) Absorption spectrum of $Ag_{31}SG_{19}$ in water. Emission (at excitation 450 nm) and Excitation spectra (at emission 705 nm (c) and 825 nm (d)) of $Ag_{31}SG_{19}$ (c) in water and (d) in ethanol (EtOH) (d).

The purity of synthesized silver nanoclusters was examined by mass spectrometry (Figure 1 a).[35, 36] A charge state distribution was observed from $[M-5H]^{5-}$ through $[M-7H]^{7-}$. Deconvolution of charge states 5 through 7 provided a mass of 9156 Da for the intact Ag cluster and was consistent with the calculated mass of $Ag_{31}SG_{19}$ (9164 Da) (see Figure S1). Experimental and simulated isotope pattern of

[M-6H]$^{6-}$ were shown in Figure S2. The pattern shape and mass position match well, though the resolution of our mass spectrometer is too low to resolve isotope pattern. The absorption spectra (Figure 1b) showed the presence of an intense visible band centred at ~490 nm, in agreement with previous findings for which a structure for Ag31 was proposed (see Fig. S3).[17] Excitation and emission spectra for $Ag_{31}SG_{19}$ nanoclusters dispersed in water and ethanol were also analyzed (Figure 1c and 1d). As already observed for Ag_{29} nanoclusters[28], the solvent-dependent emission spectra were also evidenced for $Ag_{31}SG_{19}$ NCs. Such a shift might be an indication of a stronger stabilization of the ground state than those of the excited state due to the difference in dielectric constants between H_2O and ethanol. Stability and photostability are generally important issues, that limit the applications of thiolate protected silver nanoclusters. As the, $Ag_{29}DHLA_{12}$ nanocluster was known to have poor stability due to degradation in few hours upon light exposure, [37, 38] it was not possible to study its antimicrobial activity. The emission spectra for fresh and 1-day old solutions clearly demonstrated the complete degradation of Ag_{29} in less than 24 hours (Figure 2b). On the other hand, the $Ag_{31}SG_{19}$ was found to be very stable under normal conditions and upon constant irradiation by visible laser light as confirmed by the emission spectra of fresh and 1-day old solution respectively (Figure 2a) and for absorption spectra under several dozen minutes of visible laser irradiation (Figure 2c and S4).

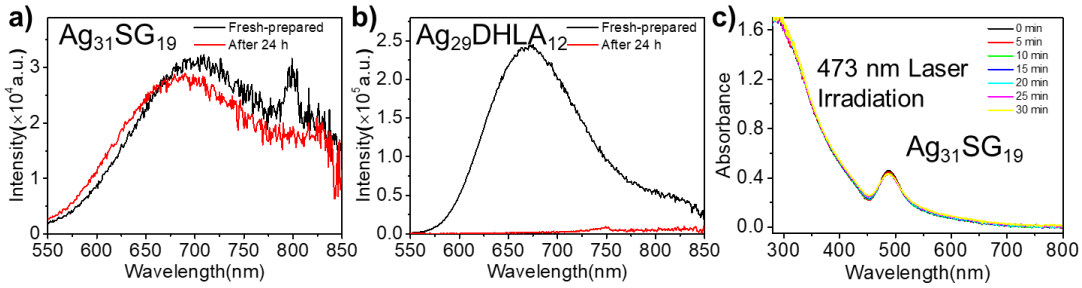

Figure 2 :Emission spectra of $Ag_{31}SG_{19}$ and $Ag_{29}DHLA_{12}$ for fresh and 24 h old solutions under normal conditions ((a) and (b)) and (c) absorption spectra of $Ag_{31}SG_{19}$ under 473 nm laser irradition for 0 to 30 minutes).

In the current study, silver nanoparticles (AgNPs) were synthesized by using a co-reduction approach, where the nucleation and growth kinetics during the synthesis process was precisely controlled and the AgNPs of average size ~6 nm were synthesized with good yield and monodispersity (Figure 3). Here, the silver nanoparticles were found to exhibit a sharp extinction peak at ~394 nm wavelength

which confirmed the surface plasmon behavior of such particles as opposed to the multi-band "molecular-like" behavior of silver nanoclusters.

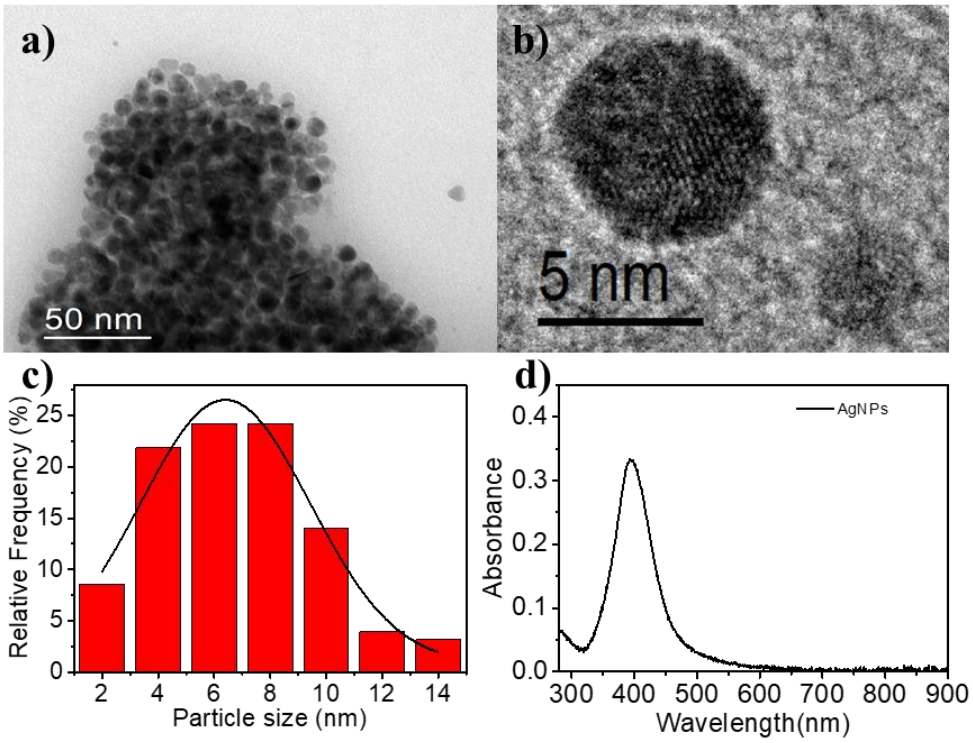

Figure 3: Characterisation of AgNPs. (a) TEM analysis, (b) HRTEM analysis, (c) size histogram, and (d) UV-VIS spectrum of plasmonic AgNPs.

3.2 ROS efficiency of $Ag_{31}SG_{19}$ in solution.

The indirect method was used to quantify the singlet oxygen generation by the photoexcited nanoclusters in solution. Here, 1,3-diphenylisobenzofuran (DPBF) has already been known to be highly reactive toward singlet oxygen resulting in the formation of endoperoxides (with different absorption properties in particular at 412 nm) and hence can be used as an optical probe.[39, 40] Both the nanoclusters and DPBF can be excited to generate and detect singlet oxygen simultaneously. Here, the generation of singlet oxygen was triggered by the excitation of the nanoclusters with a cw laser emitting at 473 nm (and also a 532 nm) with different time of exposure. Of note, no generation of singlet oxygen species occurs under darkness. The change in the absorption of DPBF was monitored over time at 412 nm.[16] Absorption spectra and the change in the absorption of DPBF monitored over time are presented in Figure 4. The rate of $^1O_2$ generation was obtained by the initial DPBF concentration

change over time (Δ[DPBF]/Δt, at shorter time where the slope has a linear behavior) divided by the concentration of the nanoclusters. To demonstrate the efficiency of Ag_{31} nanoclusters for $^1O_2$ production, we compared $^1O_2$ production by $Ag_{31}SG_{19}$ to that of the conventional dye photosensitizer new methylene blue (NMB). Under 473 nm irradiation, a superior $^1O_2$ production efficiency was observed for $Ag_{31}SG_{19}$ when compared with NMB (Table 1). The photosensitizer ability of $Ag_{31}SG_{19}$ is mainly due to its high light absorption coefficients, and long lifetime to allow high intersystem crossing efficiencies as demonstrated (Table 1). Under 532 nm irradiation (see Figure 4), a lower $^1O_2$ production efficiency ($^1O_2$ generation rate ($^1O_2$/cluster/min) = 0.980) was observed for $Ag_{31}SG_{19}$ (as compared to 473 nm irradiation). Of note, the $^1O_2$ generation rate (presented in Table 1) also depends on the absorbance of used laser light. Quantum yield of the singlet oxygen generation allows for a normalization by the absorbance at 473 nm of the cw laser. Using the protocol described in the pioneering paper[41], we were able to evaluate the quantum yield of the singlet oxygen generation (as described in supplementary materials and Figure S5). The quantum yield of $^1O_2$ generation was estimated to ~0.01-0.02.

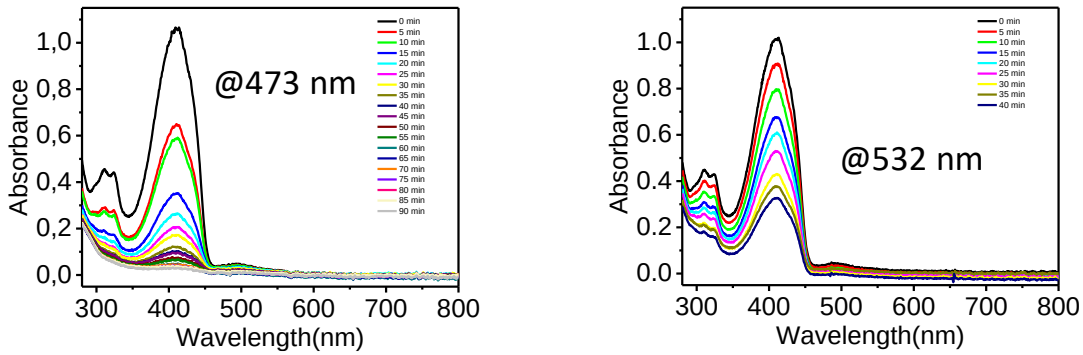

Figure 4:Absorption spectra evolution of DPBF-$Ag_{31}SG_{19}$ mixture solution under cw laser (a) 473 and (b) 532 nm irradiation.

Table 1 Singlet Oxygen generation rate by $Ag_{31}SG_{19}$ nanoclusters compared to NMB dye photosensitizer and AgNPs under cw 473 nm irradiation.

Photosensitizer	**Emission**	**Long lifetime component (ns)**	**$^1O_2$ generation rate ($^1O_2$/cluster/min) @473 nm**

$Ag_{31}SG_{19}$	705 nm	870.4±19.7 (7.2%)	3.505
NMB	652 nm	0.70 (MeOH)[42]	2.587
AgNPs			0.612

3.3 Antibacterial activity analysis of $Ag_{31}SG_{19}$

3.3.1 Agar well diffusion analysis

The antibacterial activity analysis of $Ag_{31}SG_{19}$ was carried out against *S. aureus* and *E. coli*. Here, the zone of inhibition could be observed against both *S. aureus* and *E. coli* which indicated the $Ag_{31}SG_{19}$ to have antibacterial activity. The zone of inhibition observed against *E. coli* and *S. aureus* was 15.3 ± 0.58 mm and 16.7 ± 0.58 mm respectively It was also observed that a zone of inhibition against *E. coli* was 12.3 ± 0.58 mm, whereas no zone was observed against *S. aureus* (Figure 5).

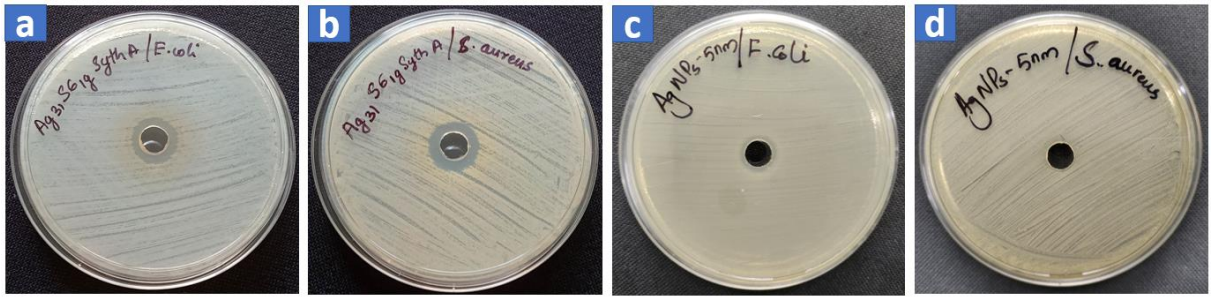

Figure 5: Antibacterial activity of (a) $Ag_{31}SG_{19}$ against E. coli, (b) $Ag_{31}SG_{19}$ against S. aureus, (c) plasmonic AgNPs against E. coli and (d) plasmonic AgNPs against S. aureus.

3.3.2 Minimum Inhibitory Concentration analysis

The MIC of $Ag_{31}SG_{19}$ against *S. aureus* and *E. coli* was determined using the standard microtiter plate assay. Here, the MIC value of $Ag_{31}SG_{19}$ against *E. coli* and *S. aureus* was found to be 0.3125 mg/ml and 0.1562 mg/ml respectively (Figure S6).

4 Discussion

In the study, the antibacterial activity of $Ag_{31}SG_{19}$ was evaluated against *E. coli* and *S. aureus* as test organisms. From the agar well diffusion analysis, $Ag_{31}SG_{19}$ (20 mg/ml) was found to have significant antibacterial activity against both bacteria with

a zone of inhibition measuring 15.3 ± 0.58 and 16.7 ± 0.58 mm respectively against *E. coli* and *S. aureus*. The size of the zone of inhibition indicates the degree of antibacterial effectiveness of $Ag_{31}SG_{19}$. However, the zone of inhibition for plasmonic AgNPs was observed to be 12.3 ± 0.58 mm against *E. coli* and no zone was observed against *S. aureus*. MIC analysis was carried out to find out the minimum concentration of $Ag_{31}SG_{19}$ required to inhibit the growth of *E. coli* and *S. aureus*. Here, the MIC of $Ag_{31}SG_{19}$ was found to be 0.1562 mg/ml against *S. aureus* and 0.3125 mg/ml against *E. coli*. Overall, the results of both the experiments suggest the $Ag_{31}SG_{19}$ to have significant antibacterial activity and hence it can have the potential to be used as an antimicrobial agent. Here, *S. aureus* was found to be more susceptible towards $Ag_{31}SG_{19}$ when compared with *E. coli*.

In the study, $Ag_{31}SG_{19}$ nanoclusters were produced with high purity for the quantitative measurements of ROS efficiencies upon visible laser irradiation. Here, the nanoclusters synthesized were found to be highly stable under daily conditions and also under continuous visible laser irradiation. This behavior is quite unique in particular when compared with the Ag_{29} nanoclusters protected by DHLA ligands. Here, $Ag_{31}SG_{19}$ presents high rates of singlet Oxygen generation in the visible range in particular upon 473 nm laser irradiation. Hence these Ag nanoclusters protected by glutathione were further used to investigate its antimicrobial efficacy against Gram-positive *S. aureus* and Gram-negative *E. coli*. Based on our findings on quantitative measurements of ROS efficiencies and photostability measurements in the solution, the primary mechanism ($^1O_2$ generation) leading to the antimicrobial activity could be a possible mechanism. Other mechanism which arise from the degradation of nanoclusters is certainly minimal here due to the high (photo)stability of $Ag_{31}SG_{19}$. However, we cannot exclude that the generation of oxidizing species (H_2O_2, radicals) upon irradiation may play a role on the antimicrobial activity of $Ag_{31}SG_{19}$. To better address this point, we used a DCF-dye, as already studied by Yuan and coworkers,[43] for probing the oxidizing agents produced following photoexcitation. We adapted this method to probe type I ROS species generated following 473 nm laser irradiation, and indeed, we confirmed that $Ag_{31}SG_{19}$ is proned to produce such oxidizing agents in addition to $^1O_2$ species. Figure S7 displays the fluorescence spectra of DCF dye without and with 10 min laser irradiation. The strong increase in fluorescence intensity is a signature of generation of type I species.

5 Conclusion

In conclusion, the antibacterial performance indicated the $Ag_{31}SG_{19}$ with superior stability to have enhanced antibacterial activity when compared to previous works using undefined glutathione protected silver nanoclusters (Table 2). The present study confirms that singlet oxygen generation produced by photo-excited $Ag_{31}SG_{19}$ nanoclusters is the key process involved in its antibacterial mechanism, while generation of oxidizing species is also involved. Singlet oxygen generation rate as well as quantum yield for $^1O_2$ generation for $Ag_{31}SG_{19}$ nanoclusters are compared to NMB dye photosensitizer under cw 473 nm and 532 nm irradiations. As singlet oxygen is considered to have rapid fatal activity and the most damaging ROS species against microorganisms, the currently studied $Ag_{31}SG_{19}$ nanoclusters can have significant antimicrobial therapeutic applications.

Table 2: Minimum Inhibitory Concentration of silver nanoclusters against E. coli and S. aureus.

Glutathione protected silver NCs	**MIC (µg/mL)**		**Ref.**
	E. coli	***S. aureus***	
$Ag_{31}SG_{19}$	312.5	156.2	Our work
Glutathione-protected Ag+-Rich NCs	450.0	358.0	Ref.[24]
$Ag_n(GSHR)_m$	1687.5	1687.5	Ref.[25]

Declaration of Competing Interest

The authors declare no conflict of interest.

Acknowledgments

We acknowledge CNRS for funding through International Emerging Actions between Institut Lumière Matière, CNRS, France and Mahatma Gandhi University, India. HY is grateful for PhD fellowships donated by the China Scholarship Council (CSC). DB is grateful for post-doc fellowship donated by Agence Nationale de la Recherche (project MANBAMM, ANR-21-CE29-0020). R.A. and H.Y. acknowledge Shanghai Science and Technology Innovation Program (22520712500) for support. We gratefully acknowledge Marion Girod (Institut des Sciences Analytiques, Villeurbanne, France) for lending us the cw lasers. MT, SK, AR and REK acknowledge KSCSTE-SRS project (307/2022/KSCSTE, Kerala) for the facility and support.

Appendix A. Supplementary data

All the data are presented in this article and the Supplementary Materials.

References

[1] T.M. Privalsky, A.M. Soohoo, J. Wang, C.T. Walsh, G.D. Wright, E.M. Gordon, N.S. Gray, C. Khosla, Prospects for Antibacterial Discovery and Development, Journal of the American Chemical Society, 143 (2021) 21127-21142. http://doi.org/10.1021/jacs.1c10200.

[2] S. Dhingra, N.A.A. Rahman, E. Peile, M. Rahman, M. Sartelli, M.A. Hassali, T. Islam, S. Islam, M. Haque, Microbial Resistance Movements: An Overview of Global Public Health Threats Posed by Antimicrobial Resistance, and How Best to Counter, Frontiers in Public Health, 8 (2020) http://doi.org/10.3389/fpubh.2020.535668.

[3] J.A. Doolan, G.T. Williams, K.L.F. Hilton, R. Chaudhari, J.S. Fossey, B.T.

Goult, J.R. Hiscock, Advancements in antimicrobial nanoscale materials and self-assembling systems, Chemical Society Reviews, 51 (2022) 8696-8755. http://doi.org/10.1039/D1CS00915J.

[4] R. Thomas, P. Jishma, S. Snigdha, K.R. Soumya, J. Mathew, E.K. Radhakrishnan, Enhanced antimicrobial efficacy of biosynthesized silver nanoparticle based antibiotic conjugates, Inorganic Chemistry Communications, 117 (2020) 107978. http://doi.org/10.1016/j.inoche.2020.107978.

[5] D. Slade, M. Radman, Oxidative Stress Resistance in *Deinococcus radiodurans*, Microbiology and Molecular Biology Reviews, 75 (2011) 133-191. http://doi.org/10.1128/MMBR.00015-10.

[6] D.J. Dwyer, M.A. Kohanski, J.J. Collins, Role of reactive oxygen species in antibiotic action and resistance, Current Opinion in Microbiology, 12 (2009) 482-489. http://doi.org/10.1016/j.mib.2009.06.018.

[7] R. Jin, Atomically precise metal nanoclusters: stable sizes and optical properties, Nanoscale, 7 (2015) 1549-1565. http://doi.org/10.1039/C4NR05794E.

[8] V. Bonacic-Koutecky, R. Antoine, Enhanced two-photon absorption of ligated silver and gold nanoclusters: theoretical and experimental assessments, Nanoscale, 11 (2019) 12436-12448. http://doi.org/10.1039/c9nr01826c.

[9] H. Qian, M. Zhu, Z. Wu, R. Jin, Quantum Sized Gold Nanoclusters with Atomic Precision, Accounts of Chemical Research, 45 (2012) 1470-1479. http://doi.org/10.1021/ar200331z.

[10] Y. Yu, B.Y.L. Mok, X.J. Loh, Y.N. Tan, Rational Design of Biomolecular Templates for Synthesizing Multifunctional Noble Metal Nanoclusters toward Personalized Theranostic Applications, Advanced Healthcare Materials, 5 (2016) 1844-1859. http://doi.org/10.1002/adhm.201600192.

[11] A. Kulesza, R. Mitric, V. Bonacic-Koutecky, B. Bellina, I. Compagnon, M. Broyer, R. Antoine, P. Dugourd, Doubly Charged Silver Clusters Stabilized by Tryptophan: Ag-4(2+) as an Optical Marker for Monitoring Particle Growth, Angewandte Chemie-International Edition, 50 (2011) 878-881. http://doi.org/10.1002/anie.201005419.

[12] G. Yang, X. Mu, X. Pan, Y. Tang, Q. Yao, Y. Wang, F. Jiang, F. Du, J. Xie, X. Zhou, X. Yuan, Ligand engineering of Au44 nanoclusters for NIR-II luminescent and photoacoustic imaging-guided cancer photothermal therapy, Chemical Science, 14 (2023) 4308-4318. http://doi.org/10.1039/D2SC05729H.

[13] G. Yang, X. Pan, W. Feng, Q. Yao, F. Jiang, F. Du, X. Zhou, J. Xie, X. Yuan, Engineering Au44 Nanoclusters for NIR-II Luminescence Imaging-Guided Photoactivatable Cancer Immunotherapy, ACS Nano, 17 (2023) 15605-15614. http://doi.org/10.1021/acsnano.3c02370.

[14] G. Yang, Z. Wang, F. Du, F. Jiang, X. Yuan, J.Y. Ying, Ultrasmall Coinage Metal Nanoclusters as Promising Theranostic Probes for Biomedical Applications, Journal of the American Chemical Society, 145 (2023) 11879-11898. http://doi.org/10.1021/jacs.3c02880.

[15] H. Kawasaki, S. Kumar, G. Li, C. Zeng, D.R. Kauffman, J. Yoshimoto, Y. Iwasaki, R. Jin, Generation of Singlet Oxygen by Photoexcited Au25(SR)18 Clusters, Chemistry of Materials, 26 (2014) 2777-2788. http://doi.org/10.1021/cm500260z.

[16] R. Ho-Wu, S.H. Yau, T. Goodson, III, Efficient Singlet Oxygen Generation in Metal Nanoclusters for Two-Photon Photodynamic Therapy Applications, The Journal of Physical Chemistry B, 121 (2017) 10073-10080. http://doi.org/10.1021/acs.jpcb.7b09442.

[17] F. Bertorelle, R. Hamouda, D. Rayane, M. Broyer, R. Antoine, P. Dugourd, L. Gell, A. Kulesza, R. Mitrić, V. Bonačić-Koutecký, Synthesis, characterization and optical properties of low nuclearity liganded silver clusters: Ag31(SG)19 and Ag15(SG)11, Nanoscale, 5 (2013) 5637-5643. http://doi.org/10.1039/C3NR00677H.

[18] K. Zheng, M.I. Setyawati, D.T. Leong, J. Xie, Antimicrobial silver nanomaterials, Coordination Chemistry Reviews, 357 (2018) 1-17. http://doi.org/10.1016/j.ccr.2017.11.019.

[19] X. Yuan, M.I. Setyawati, A.S. Tan, C.N. Ong, D.T. Leong, J. Xie, Highly luminescent silver nanoclusters with tunable emissions: cyclic reduction–decomposition synthesis and antimicrobial properties, NPG Asia Materials, 5 (2013) e39-e39. http://doi.org/10.1038/am.2013.3.

[20] Y. Chen, L. Ren, L. Sun, X. Bai, G. Zhuang, B. Cao, G. Hu, N. Zheng, S. Liu, Amphiphilic silver nanoclusters show active nano–bio interaction with compelling antibacterial activity against multidrug-resistant bacteria, NPG Asia Materials, 12 (2020) 56. http://doi.org/10.1038/s41427-020-00239-y.

[21] Y. Zheng, M. Wei, H. Wu, F. Li, D. Ling, Antibacterial metal nanoclusters, Journal of Nanobiotechnology, 20 (2022) 328. http://doi.org/10.1186/s12951-022-01538-y.

[22] B.G. Vijayakumar, D. Ramesh, K. Santhosh Manikandan, M. Theresa, A. Sethumadhavan, V.B. Priyadarisini, E.K. Radhakrishnan, M. Mani, T. Kannan, Chitosan with pendant (E)-5-((4-acetylphenyl)diazenyl)-6-aminouracil groups as synergetic antimicrobial agents, Journal of Materials Chemistry B, 10 (2022) 4048-4058. http://doi.org/10.1039/D2TB00240J.

[23] R. Thomas, K.R. Soumya, J. Mathew, E.K. Radhakrishnan, Inhibitory effect of silver nanoparticle fabricated urinary catheter on colonization efficiency of Coagulase Negative Staphylococci, Journal of Photochemistry and Photobiology B: Biology, 149 (2015) 68-77. http://doi.org/10.1016/j.jphotobiol.2015.04.034.

[24] X. Yuan, M.I. Setyawati, D.T. Leong, J. Xie, Ultrasmall Ag+-rich nanoclusters as highly efficient nanoreservoirs for bacterial killing, Nano Research, 7 (2014) 301-307. http://doi.org/10.1007/s12274-013-0395-6.

[25] K. Wang, Y. Wu, H. Li, M. Li, D. Zhang, H. Feng, H. Fan, Synthesis, characterization and antimicrobial activity of silver nanoparticles: Agn(NALC)m and Agn(GSHR)m, RSC Advances, 4 (2014) 5130-5135. http://doi.org/10.1039/C3RA46568C.

[26] R. Antoine, Supramolecular Gold Chemistry: From Atomically Precise

Thiolate-Protected Gold Nanoclusters to Gold-Thiolate Nanostructures, Nanomaterials, 10 (2020) 377. http://doi.org/10.3390/nano10020377.

[27] A. Soleilhac, X. Dagany, P. Dugourd, M. Girod, R. Antoine, Correlating Droplet Size with Temperature Changes in Electrospray Source by Optical Methods, Analytical Chemistry, 87 (2015) 8210-8217. http://doi.org/10.1021/acs.analchem.5b00976.

[28] I. Russier-Antoine, F. Bertorelle, R. Hamouda, D. Rayane, P. Dugourd, Z. Sanader, V. Bonacic-Koutecky, P.-F. Brevet, R. Antoine, Tuning Ag-29 nanocluster light emission from red to blue with one and two-photon excitation, Nanoscale, 8 (2016) 2892-2898. http://doi.org/10.1039/c5nr08122j.

[29] S. Agnihotri, S. Mukherji, S. Mukherji, Size-controlled silver nanoparticles synthesized over the range 5–100 nm using the same protocol and their antibacterial efficacy, RSC Adv., 4 (2014) 3974-3983. http://doi.org/10.1039/c3ra44507k.

[30] P. Mulvaney, M. Giersig, A. Henglein, Electrochemistry of multilayer colloids: preparation and absorption spectrum of gold-coated silver particles, The Journal of Physical Chemistry, 97 (1993) 7061-7064. http://doi.org/10.1021/j100129a022.

[31] X. Chen, Z. Zhong, Z. Xu, L. Chen, Y. Wang, 2',7'-Dichlorodihydrofluorescein as a fluorescent probe for reactive oxygen species measurement: Forty years of application and controversy, Free Radic Res, 44 (2010) 587-604. http://doi.org/10.3109/10715761003709802.

[32] H. Zhu, N. Liu, Z. Wang, Q. Xue, Q. Wang, X. Wang, Y. Liu, Z. Yin, X. Yuan, Marrying luminescent Au nanoclusters to TiO2 for visible-light-driven antibacterial application, Nanoscale, 13 (2021) 18996-19003. http://doi.org/10.1039/D1NR05503H.

[33] W. Jakubowski, G. Bartosz, 2,7-dichlorofluorescin oxidation and reactive oxygen species: what does it measure?, Cell Biol Int, 24 (2000) 757-760. http://doi.org/10.1006/cbir.2000.0556.

[34] E. Saied, A.E. Mekky, A.A. Al-Askar, A.F. Hagag, A.A. El-bana, M. Ashraf, A. Walid, T. Nour, M.M. Fawzi, A.A. Arishi, A.H. Hashem, Aspergillus terreus-Mediated Selenium Nanoparticles and Their Antimicrobial and Photocatalytic Activities, Crystals, 13 (2023) 450. http://doi.org/10.3390/cryst13030450.

[35] C. Comby-Zerbino, X. Dagany, F. Chirot, P. Dugourd, R. Antoine, The emergence of mass spectrometry for characterizing nanomaterials. Atomically precise nanoclusters and beyond, Materials Advances, 2 (2021) 4896-4913. http://doi.org/10.1039/d1ma00261a.

[36] A. Soleilhac, F. Bertorelle, C. Comby-Zerbino, F. Chirot, N. Calin, P. Dugourd, R. Antoine, Size Characterization of Glutathione-Protected Gold Nanoclusters in the Solid, Liquid and Gas Phases, The Journal of Physical Chemistry C, 121 (2017) 27733-27740. http://doi.org/10.1021/acs.jpcc.7b09500.

[37] M. van der Linden, A. Barendregt, A.J. van Bunningen, P.T.K. Chin, D. Thies-Weesie, F.M.F. de Groot, A. Meijerink, Characterisation, degradation and

regeneration of luminescent Ag29 clusters in solution, Nanoscale, 8 (2016) 19901-19909. http://doi.org/10.1039/C6NR04958C.

[38] H. Fakhouri, E. Salmon, X. Wei, S. Joly, C. Moulin, I. Russier-Antoine, P.-F. Brevet, X. Kang, M. Zhu, R. Antoine, Effects of Single Platinum Atom Doping on Stability and Nonlinear Optical Properties of Ag29 Nanoclusters, The Journal of Physical Chemistry C, 126 (2022) 21094-21100. http://doi.org/10.1021/acs.jpcc.2c06836.

[39] T. Entradas, S. Waldron, M. Volk, The detection sensitivity of commonly used singlet oxygen probes in aqueous environments, Journal of Photochemistry and Photobiology B: Biology, 204 (2020) 111787. http://doi.org/10.1016/j.jphotobiol.2020.111787.

[40] H. Fakhouri, M.P. Bakulić, I. Zhang, H. Yuan, D. Bain, F. Rondepierre, P.-F. Brevet, Ž.S. Maršić, R. Antoine, V. Bonačić-Koutecký, D. Maysinger, Ligand impact on reactive oxygen species generation of Au10 and Au25 nanoclusters upon one- and two-photon excitation, Communications Chemistry, 6 (2023) 97. http://doi.org/10.1038/s42004-023-00895-5.

[41] D.M. Marin, S. Payerpaj, G.S. Collier, A.L. Ortiz, G. Singh, M. Jones, M.G. Walter, Efficient intersystem crossing using singly halogenated carbomethoxyphenyl porphyrins measured using delayed fluorescence, chemical quenching, and singlet oxygen emission, Physical Chemistry Chemical Physics, 17 (2015) 29090-29096. http://doi.org/10.1039/C5CP04359J.

[42] F. Ronzani, A. Trivella, E. Arzoumanian, S. Blanc, M. Sarakha, C. Richard, E. Oliveros, S. Lacombe, Comparison of the photophysical properties of three phenothiazine derivatives: transient detection and singlet oxygen production, Photochemical & Photobiological Sciences, 12 (2013) 2160-2169. http://doi.org/10.1039/C3PP50246E.

[43] N. Liu, Y. Wang, Z. Wang, Q. He, Y. Liu, X. Dou, Z. Yin, Y. Li, H. Zhu, X. Yuan, Conjugating AIE-featured AuAg nanoclusters with highly luminescent carbon dots for improved visible-light-driven antibacterial activity, Nanoscale, 14 (2022) 8183-8191. http://doi.org/10.1039/D2NR01550A.